Accepted Manuscript

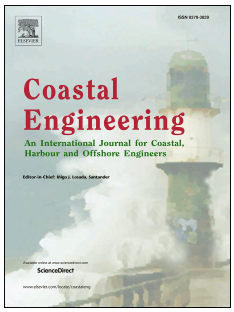

Resolving combined wave-current fields from measurements using interior point optimization

S. Draycott, A.C. Pillai, D.M. Ingram, L. Johanning

PII: S0378-3839(18)30378-8

DOI: https://doi.org/10.1016/j.coastaleng.2019.03.008

Reference: CENG 3483

To appear in: *Coastal Engineering*

Received Date: 10 August 2018

Revised Date: 31 January 2019

Accepted Date: 18 March 2019

Please cite this article as: Draycott, S., Pillai, A.C., Ingram, D.M., Johanning, L., Resolving combined wave-current fields from measurements using interior point optimization, *Coastal Engineering* (2019), doi: https://doi.org/10.1016/j.coastaleng.2019.03.008.

Resolving Combined Wave-Current Fields from Measurements using Interior Point Optimization

S. Draycott[a,*], A.C. Pillai[b], D.M.Ingram[a], L.Johanning[b]

[a]*School of Engineering, Institute for Energy Systems, The University of Edinburgh, Edinburgh, UK, EH9 3DW*
[b]*College of Engineering, Mathematics and Physical Sciences, University of Exeter, Penryn Campus, UK, TR10 9FE*

Abstract

Complex wave and wave-current conditions exist in the natural world, and are increasingly emulated in advanced experimental facilities to de-risk the deployment, operation and maintenance of offshore structures and renewable energy devices. This can include combinations of ocean swell, multi-directional wind-driven seas, and reflected wave conditions interacting with a current field. It is vital to understand the full nature of these potentially hazardous conditions so they can be properly simulated in numerical models, to contextualize measurements made in field, and experimental programmes. Here, a numerical framework is presented for isolating both the wave systems and the mean current velocities from measured data using an interior point optimizer.

A developed frequency domain solver is used to resolve, from experimentally obtained wave gauge measurements, two opposing wave systems on a collinear current, and used to effectively isolate the wave systems and predict the current velocity using only wave gauge measurements. Thirty five test cases are considered; consisting of five wave spectra interacting with seven different current velocities ranging from $-0.3\,\mathrm{m\,s^{-1}}$ to $0.3\,\mathrm{m\,s^{-1}}$. Comparisons between the theoretical and derived wave numbers and current velocities show good agreement and the performance of the method is similar to that of existing methodologies while requiring no a priori knowledge of the current velocity impacting the wave field required.

Although results are presented for the collinear problem, the presented method can be applied to a wide range of wave and current combinations, and provides a useful tool for increasing understanding of both ocean and experimental conditions.

Keywords:
Wave-Current Interactions, Wave Reflection Analysis, Tank Testing, Interior-Point Optimization, Non-linear Programming

1. Introduction

Combinations of waves and currents exist in a wide range of coastal and ocean locations. They interact with each other to create complex, potentially hazardous conditions. Wave kinematics are

*Corresponding author
Email address: S.Draycott@ed.ac.uk (S. Draycott)

significantly altered by the presence of current (see e.g. Jonsson (1970, 1990); Masson (1996); Smith (1997)) whilst the current, including the vertical profile, is also modified by the presence of wave-induced velocities (Olabarrieta et al., 2010). This combined wave-current field will largely determine the loading and response of offshore structures, vessels, and devices (Bruserud et al., 2018). As such, it is critical to measure, test within, and understand likely combinations of wave-current conditions, in order to ensure that engineering systems are designed appropriately.

It can be challenging to measure complex wave-current conditions, either for laboratory scale experiments or full-scale ocean instrument deployments. This becomes particularly difficult where there are multiple wave systems, as single or pseudo-single component measurement systems cannot infer directionality. Even for multi-component measurement systems, this can be challenging due to inherent assumptions in the analysis (see Benoit et al. (1997) for details), and the resulting outputs are phase-averaged. The existence of multiple wave systems on a current is a fairly common occurrence in tidal channels, where remnants of a storm co-exist with a near-opposing wave system. For example, the Pentland Firth in Scotland is exposed to the North Sea on the East and the North Atlantic to the West (see De Dominicis et al. (2017)).

Combinations of wave systems on a current are not limited to tidal channels: multi-modal sea states are common (Rodríguez and Guedes Soares, 1999) and will often exist on ocean currents; and wave reflection from natural or man-made coastline (Dickson et al., 1995; Chen et al., 2006) will also result in multiple effective wave systems. In laboratory experiments, two or more wave-current systems will exist when either trying to emulate these conditions at scale, or in the presence of undesired reflections from tank walls or models (see Draycott et al. (2016)). Whether focusing on field measurements or laboratory experiments, it is critical to understand the conditions present so that design cases can be formulated and simulated, and measurements can be properly contextualized.

Here we present a numerical framework that is able to resolve a wide range of wave and wave-current conditions. An interior point optimization solver, IPOPT (Wright, 2005; Wächter et al., 2015), is used, in the frequency domain, to solve for unknown wave and current parameters by minimizing the sum of square errors between measurements and a proposed wave or wave-current field formulation. This error function, based on linear wave theory in the present case, serves as the objective function to the optimization problem and can be modified to solve specific problems using the same solution approach and solver. This approach can therefore be readily adapted to operate on various wave parameters depending on the measurements available. In this paper we apply the presented framework to solve the complex problem of two wave fields on a current (assumed unknown) propagating in opposing directions. Surface elevation data was measured in the combined wave-current basin at the FloWave Ocean Energy Research Facility, Edinburgh, UK (Ingram et al., 2014). The tool is used to isolate the wave systems and estimate the current velocity with wave gauge data alone; by virtue of solving for the current affected wavenumbers directly. Though applied to this problem due to its relevance and applicability in both field and experimental work, it is envisioned that the same framework can be applied to resolve wave systems and current in a number of other scenarios, such as:

1. isolating two opposing wave systems i.e. standard reflection analysis (see Goda and Suzuki (1976); Zelt and Skjelbreia (1992))

2. isolating more than two wave systems e.g. multiple incident and reflected wave fields
3. measuring directional spectra⋆ and inferring current velocity
4. isolating combinations of directional spectra⋆
5. isolating combinations of directional spectra⋆ on current, and inferring the current velocity

⋆ *Only applicable to experimentally obtained data, where the single-summation method has been used to generate the directional sea states.*

The article is laid out as follows: Section 2 describes the theory related to wave-current interaction and interior point optimization. The methodology used to solve the aforementioned problem is detailed in Section 3, whilst also describing the numerical framework developed to solve for analogous problems. The experimental set-up is described in Section 4, results presented in Section 5, and further discussion in Section 6. Concluding remarks are offered in Section 7.

2. Theory

The theory presented in this section is limited to two wave systems, and focuses on problems incorporating current. It is, however, trivial to modify the presented formulae to include additional or fewer wave systems, or to ignore the current, if appropriate. The subsequent ability to solve a given formulation depends on the number of gauges together with their respective separations.

All the equations presented below are written in terms of surface elevation measurements to correspond to the experiments. A similar procedure, however, can be implemented for any wave signal e.g. pressure, velocity, acceleration, slope etc. Equally, a combination of measurement types may be used. Transfer functions, such as those presented in Benoit et al. (1997), may be used to convert all measurements to equivalent surface elevations, simplifying the solution procedure.

2.1. Wave-current Interaction

Current alters the form of waves significantly, modifying the height, wavenumbers, and associated velocities. For spatial measurements of surface elevation the key unknown is the wavenumber, as this determines the phase relationship between different spatial locations (gauges). Without the presence of current, wavenumber is related to angular frequency via Eq. (1). A modified version is required for problems with current due to the Doppler shift, and is described in Jonsson (1990). It is worth noting that this simple formulation assumes that the current field is steady and uniform.

$$\omega = \sqrt{g k_0 \tanh k_0 h} \tag{1}$$

$$\omega - k_1 U \cos\beta = \sqrt{g k_1 \tanh k_1 h} \tag{2}$$

where β is the relative angle between the wave and current fields, and $\beta = 0$ for waves travelling on a following current. ω_i is the angular frequency, k_1 and k_0 are the current modified and current unmodified wavenumbers respectively, and h is the water depth.

For waves opposing current this has the effect of steepening the waves; a combined effect of increased wave height and reduced wavelength. The opposite is true for waves following a current. An example of this interaction is depicted in Fig. 1, whereby a monochromatic wave is shown propagating onto an opposing current field.

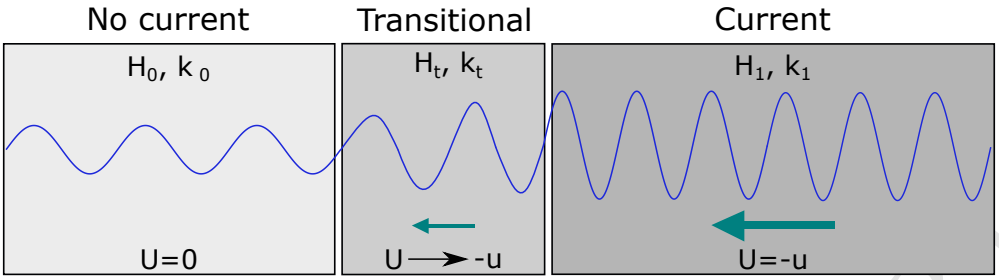

Figure 1: Diagram showing wave propagating from region of no current to a region with current. Change in wave height and wavelength (wavenumber) due to interaction with current field indicated. Example shown with opposing current (negative u) where wave height increases and wavelength decreases (Draycott et al., 2018)

2.2. *Spatial Interaction of Multiple Wave-Current Fields*

Assuming linear wave theory (Krogstad, 2000), the surface elevation time-series at an $[x, y]$ location can be described as a double sum of sinusoidal wave components over frequency and direction:

$$\eta(x, y, t) = \sum_{j\in\mathbb{F}} \sum_{m=0}^{N_\theta} a_{j,m} \sin(k_{1,j,m}(x\cos\theta_{j,m} + y\sin\theta_{j,m}) - \omega_i t + \Phi_{j,m}) \tag{3}$$

where $\mathbb{F}$ is the set of frequency components, N_θ is the number of directional components, $a_{j,m}$ and $k_{1,j,m}$ are the component wave amplitude and wavenumber for the frequency-angle combination (j, m), and $\Phi_{j,m}$ is the corresponding phase referenced at $t = 0$ and $[x, y] = 0$.

In the frequency domain, the equivalent formulation for $A_{j,p}$, the Fourier component at frequency j and wave gauge p in the set of wavegauges $\mathbb{P}$, is as follows:

$$A_{j,p} = \sum_{m=0}^{N_\theta} a_{j,m} e^{ik_{1,j,m}(x_p\cos\theta_{j,m} + y_p\sin\theta_{j,m})} \tag{4}$$

where $a_{j,m}$ is complex and includes the phase, $\Phi_{j,m}$.

These describe sea states with an arbitrary number of frequency components, and an arbitrary number of directional components for each frequency. In experimental work it is typical, and indeed advisable, to have one directional component for each frequency to avoid phase locking (Jefferys, 1987) and the creation of a non-ergodic wave field. Hence, the single summation method of directional wave generation is utilized (Miles and Funke, 1989). This reduces Eq. (4) to:

$$A_{j,p} = a_j e^{ik_{1,j}(x_p\cos\theta_j + y_p\sin\theta_j)} \tag{5}$$

which is then a valid linear wave theory approximation for ocean data and tank experiments where unidirectionality can be assumed, and for all basin experiments which utilise single summation directional wave generation.

When there are two wave systems (at each frequency), as described in Section 1 (i.e. two opposing systems in a channel, reflected wave systems etc.) it is necessary to extend this formulation,

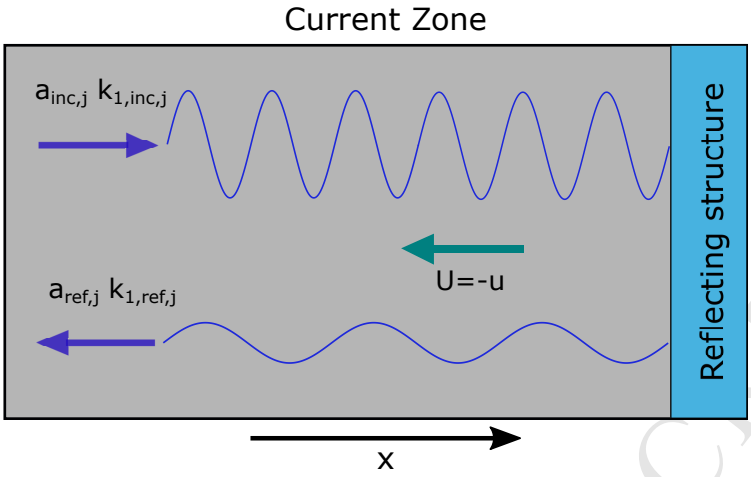

Figure 2: The wave field in the measurement (current) zone is made up of incident and reflected components from a structure. In the diagram the reflecting structure is shown inside the current zone but could equally be outside. Highlights that for a given frequency component, j, that there is exist two wavenumbers and amplitudes for each frequency. Shown here with opposing current (negative U) where wavelength decreases for incident, and increases for reflected wave components (Draycott et al., 2018)

as follows:

$$A_{j,p} = a_{inc,j} e^{ik_{1,inc,j}(x_p \cos\theta_{inc,j} + y_p \sin\theta_{inc,j})} + a_{ref,j} e^{ik_{1,ref,j}(x_p \cos\theta_{ref,j} + y_p \sin\theta_{ref,j})} \tag{6}$$

where $a_{inc,j}$ and $a_{ref,j}$ refer to the 'incident' and 'reflected' wave fields, and θ_{inc} and θ_{ref} refer to their respective propagation directions. For collinear cases, where wave systems follow and oppose the current field Eq. (7) is applicable to both ocean and tank data. The terms incident and reflected are used here, as are appropriate descriptors for the experimental work, however, they essentially refer to two wave systems travelling in different directions.

$$A_{j,p} = a_{inc,j} e^{ik_{1,inc,j}x_p} + a_{ref,j} e^{-ik_{1,ref,j}x_p} \tag{7}$$

This problem is explored in this work as it is a valid representation for a variety of ocean and experimental scenarios; in particular tidal channels with multiple wave systems, and incident and reflected (or left and right travelling) wave fields in experimental facilities. Fig. 2 depicts this wave field, showing that when current is present two wavenumbers, amplitudes and phases exist for every frequency component.

2.3. Interior Point Optimization

In order to resolve the parameters of multiple wave systems given in Eq. (6) or Eq. (7) an optimization based approach is proposed in the present work. Using an optimization framework allows the problem to be formulated as one in which the optimizer seeks to identify the wave parameters such that the difference between the wave systems that these estimated parameters describe and the measurements is minimized. Optimization algorithms seek to identify the best possible solution amongst all those available. All optimization algorithms require a representation of the problem with respect to an evaluation function which judges the relative quality of the proposed solutions. A search algorithm is then deployed to minimize or maximize this objective function (Burke and

Kendall, 2013). Parameter estimation, those problems which seek to fit a model to measurements, for a system involving many variables which may have complex relationships to one another can be addressed using an optimization approach in which the objective function represents an error function between the model and the measurements. For such approaches, many optimization algorithms may be relevant; for problems with complex relationships between the parameters being estimated, in this case the parameters describing the wave systems, with functions which cannot be easily differentiated, heuristic algorithms such as the genetic algorithm or particle swarm would be appropriate. If, however, the problem can be formulated as a convex non-linear programming function with differentiable objectives and constraints, then gradient based algorithms such as interior point methods would offer a more efficient means of solving the problem (Rao, 2009; Wächter and Biegler, 2006; Wright, 2005).

Interior point methods are a class of algorithms used to solve linear and non-linear convex optimization problems based on traversing the feasible space (i.e. the interior space) of a constrained optimization problem (Wright, 2005). These algorithms are gradient based optimization algorithms which operate by computing the first and second derivatives, or approximations of these, of the objective and constraint functions in order to converge to the optimal solution (Ye, 1997). As they are gradient based methods, they can converge to local solutions depending on the initialization of the optimizer and are not guaranteed to converge to a global solution, however, they can often demonstrate better convergence properties than a global optimizer for a well structured problem with defined derivatives (Wächter et al., 2015).

IPOPT introduced by Wächter (2002) and further developed in Wächter et al. (2015) is an interior point optimization algorithm which designed for large-scale continuous non-linear single objective optimization problems. IPOPT solves non-linear optimization problems in the general form:

$$\begin{aligned} \min \quad & f(x) \\ \text{s.t.} \quad & g^L \leq g(x) \leq g^U \\ & x^L \leq x \leq x^U \end{aligned}$$

where x is the vector of decision variables; $f(x)$ is the convex objective function to be minimized; g^L and g^U are respectively the lower and upper bounds on the constraint function $g(x)$; and x^L and x^U are respectively the lower and upper bounds on the decision variables.

3. Methodology

3.1. Isolating Multiple Wave-Current Fields using Wave Gauge Measurements

Typically it is desirable to have a greater number of wave gauges (with useful separations) than degrees of freedom, and hence the system is over-resolved. To resolve the wave systems in an over-determined system, the total discrepancy between the measured, B, and theoretical Fourier coefficients, A, is minimized. This is described by Eq. (8) for each frequency component (j) and every wave gauge (p) in the set of wave gauges ($\mathbb{P}$).

$$\epsilon_{j,p} = A_{j,p} - B_{j,p} \tag{8}$$

where $A_{j,p}$ is any theoretical formulation corresponding to the expected physical conditions. For the experiments presented in Section 5, Eq. (7) is used. The objective function, E_j, to minimize is based on minimizing the weighted sum of square errors across all wave gauges:

$$E_j = \sum_{p \in \mathbb{P}} W_{j,p} \epsilon_{j,p} \epsilon^*_{j,p} \tag{9}$$

where $W_{j,p}$ is the weighting function applied for a given wave gauge and frequency, and can be used to improve the quality of the results. The complex-conjugate is denoted by *. The weighting function used here is the same as that presented in Zelt and Skjelbreia (1992), based on the ratio of the gauge separations to the k values at frequency j, Although the k values are treated as unknown for our problem, the current unmodified values are used in the calculation of the weighting function to provide effective results to the overall problem.

The number of variables to solve for will depend on the problem in question. For the present experimental work, the propagation directions of the two systems and current are known and the wave systems are assumed to be collinear to the current. Hence, the complex amplitudes $a_{inc,j}$, $a_{ref,j}$, along with the two wavenumbers $k_{1,inc,j}$ and $k_{1,ref,j}$ are the parameters of interest. This therefore does not use Eq. (2) to determine the current modified wave numbers knowing the magnitude of the current velocity, but instead allows the current velocity to be calculated from the wavenumbers identified by the solver.

3.2. Estimating Current Velocity

The generalized solver developed here is capable of isolating the wave systems without any prior knowledge of the current speed or wavenumbers. From the estimated parameters, the wavenumbers calculated for each of the wave systems enables estimates of the current velocity to be obtained by rearranging Eq. (2). An estimate is obtained for each frequency component, for each wave system:

$$U_j = \frac{\omega_j - \sqrt{g k_{1,j} \tanh(k_{1,j} h)}}{k_{1,j} \cos\beta} \tag{10}$$

where β is the separation angle between frequency component j of the wave system and the current. The U_j values are essentially the representative current for the frequency component of interest. Higher frequencies will therefore provide estimates of the the current closer to the surface due to their relative depth attenuation. As the vertical shear profile in FloWave approximately follows a $\frac{1}{15}^{th}$ power law (Sutherland et al., 2017), the difference between the mean velocity experienced by the waves and the depth averaged velocity should be relatively small.

Due to more stable results noted for the dominant wave system, the total current velocity estimate is obtained by weighting frequency-dependent estimates of U from the incident system by the incident amplitudes:

$$U_{total} = \frac{\sum_{j \in \mathbb{F}} U_j \, a_{inc,j}}{\sum_{j \in \mathbb{F}} a_{inc,j}} \tag{11}$$

3.3. Formulation of Optimization Problem

IPOPT allows any parameters of interest regarding the wave systems to be resolved using the same overarching methodology. To accomplish this the specific decision variables, objectives, and constraints must be representable in the general from given in Section 2. It is important that the objective function, generally an error function to be minimized for parameter estimation problems, includes contributions from each of the decision variables. Likewise it is important that the constraint set correctly describes the relationships between the parameters and their limitations. In the section that follows, the optimization problem for resolving two coinciding wave systems in the presence of current is formulated in full, and the solution approach using IPOPT is described. Though the formulation below is specific to the problem at hand, the general approach demonstrated can be used to solve for any parameters of interest in the combined wave-current system.

To solve for the wave systems in the present over-determined system, the problem is formulated as a minimization problem wherein the optimization algorithm decision variables represent the parameters of the wave systems. In this way, by minimizing an objective function based on the merit function given in Eq. (9), the optimization algorithm will determine the relevant parameters which define the wave and current systems. This objective is given in Eq. (12).

The decision variables represent the complex amplitudes given by $a_{inc,j}$, $a_{ref,j}$, along with the two wavenumbers $k_{1,inc,j}$ and $k_{1,ref,j}$ for the two wave systems. To conform with linear wave theory, a constraint was introduced to ensure that the wavenumbers increase with frequency (Eqs. (13) and (14)).

Unlike the wavenumbers, the complex amplitudes are not expected to increase with frequency and as such no further constraints are placed on the complex amplitudes. Furthermore, all the decision variables were bounded as given in Eqs. (17) to (22) based on the theoretical ranges that these values could occupy. The current affected wavenumbers were assigned an upper bound of $3 \times k_0$ in order to aid the convergence behaviour of the optimization process.

As IPOPT is only developed for real valued functions and variables, the complex parameters are divided into separate real and imaginary components in order for all the decision variables to be real valued. This leads to the following representation of the decision variables:

- α_j: the real component of the complex amplitude of the incident wave spectra at frequency j $\left(\mathrm{Re}\left(a_{inc,j}\right)\right)$
- γ_j: the imaginary component of the complex amplitude of the incident wave spectra at frequency j $\left(\mathrm{Im}\left(a_{inc,j}\right)\right)$
- ζ_j: the real component of the complex amplitude of the reflected wave spectra at frequency j $\left(\mathrm{Re}\left(a_{ref,j}\right)\right)$
- μ_j: the imaginary component of the complex amplitude of the reflected wave spectra at frequency j $\left(\mathrm{Im}\left(a_{ref,j}\right)\right)$
- $k_{1,inc,j}$: the wavenumber of the incident wave spectra at frequency j

- $k_{1,ref,j}$: the wavenumber of the reflected wave spectra at frequency j

$$\text{minimize} \quad E = \sum_{j\in\mathbb{F}} \sum_{p\in\mathbb{P}} W_{j,p}\epsilon_{j,p}\epsilon^*_{j,p} \tag{12}$$

$$\begin{aligned}
\text{subject to} \quad & k_{1,inc,j} \geq k_{1,inc,j-1} && \forall j \in \mathbb{F} && (13)\\
& k_{1,ref,j} \geq k_{1,ref,j-1} && \forall j \in \mathbb{F} && (14)\\
& a_{inc,j} = \alpha_j + i\gamma_j && \forall j \in \mathbb{F} && (15)\\
& a_{ref,j} = \zeta_j + i\mu_j && \forall j \in \mathbb{F} && (16)\\
& -1 \leq \alpha_j \leq 1 && \forall j \in \mathbb{F} && (17)\\
& -1 \leq \gamma_j \leq 1 && \forall j \in \mathbb{F} && (18)\\
& -1 \leq \zeta_j \leq 1 && \forall j \in \mathbb{F} && (19)\\
& -1 \leq \mu_j \leq 1 && \forall j \in \mathbb{F} && (20)\\
& 0 \leq k_{1,inc,j} \leq 3 \cdot k_{0,j} && \forall j \in \mathbb{F} && (21)\\
& 0 \leq k_{1,ref,j} \leq 3 \cdot k_{0,j} && \forall j \in \mathbb{F} && (22)
\end{aligned}$$

In the event that the current direction is known relative to the incident wave field (i.e. if the waves are following or opposing current), additional constraints can be introduced in line with the theory shown in Fig. 1 to aid the convergence behaviour. The inclusion of these constraints does not impact the resolved wave parameters, but merely the time taken by the optimizer to identify these. These constraints represent:

- wavenumber of the wave system opposing currents are less than the current unaffected wavenumbers (Eqs. (23) and (25); and
- wavenumber of the wave system following currents are greater than the current unaffected wavenumbers (Eqs. (24) and (26).

$$\begin{aligned}
& k_{1,inc,j} \geq k_{0,j} && \forall U < 0; \forall j \in \mathbb{F} && (23)\\
& k_{1,inc,j} \leq k_{0,j} && \forall U > 0; \forall j \in \mathbb{F} && (24)\\
& k_{1,ref,j} \leq k_{0,j} && \forall U < 0; \forall j \in \mathbb{F} && (25)\\
& k_{1,ref,j} \geq k_{0,j} && \forall U > 0; \forall j \in \mathbb{F} && (26)
\end{aligned}$$

IPOPT as a gradient based optimization algorithm requires the first derivative of both the objective function and the constraint functions (referred to as the gradient of the objective and Jacobian respectively). Where these are not defined, a numerical differentiation scheme is used to approximate the derivatives. Numerical differentiation, however, tends to scale poorly as the problem size increases and can become computationally expensive (Wächter and Biegler, 2006).

Given that the frequency component of each the decision variables are combined linearly in the objective function, the gradient of the objective can be treated independently for each frequency component:

$$\frac{\partial E}{\partial \alpha_j} = \sum_{p\in\mathbb{P}} W_{j,p} e^{ik_{1,inc,j}x_p}\left[\left(\alpha_j+\gamma_j i\right)e^{ik_{1,inc,j}x_p}+\left(\zeta_j+\mu_j i\right)e^{-ik_{1,ref,j}x_p}-B_{j,p}\right]^* + W_{j,p}\left(e^{ik_{1,inc,j}x_p}\right)^*\left[\left(\alpha_j+\gamma_j i\right)e^{ik_{1,inc,j}x_p}+\left(\zeta_j+\mu_j i\right)e^{-ik_{1,ref,j}x_p}-B_{j,p}\right] \tag{27}$$

$$\frac{\partial E}{\partial \gamma_j} = \sum_{p\in\mathbb{P}} W_{j,p} ie^{ik_{1,inc,j}x_p}\left[\left(\alpha_j+\gamma_j i\right)e^{ik_{1,inc,j}x_p}+\left(\zeta_j+\mu_j i\right)e^{-ik_{1,ref,j}x_p}-B_{j,p}\right]^* + W_{j,p}\left(ie^{ik_{1,inc,j}x_p}\right)^*\left[\left(\alpha_j+\gamma_j i\right)e^{ik_{1,inc,j}x_p}+\left(\zeta_j+\mu_j i\right)e^{-ik_{1,ref,j}x_p}-B_{j,p}\right] \tag{28}$$

$$\frac{\partial E}{\partial k_{1,inc,j}} = \sum_{p\in\mathbb{P}} W_{j,p}\left[\left(\alpha_j+\gamma_j i\right)ix_p e^{ik_{1,inc,j}x_p}\right]\left[\left(\alpha_j+\gamma_j i\right)e^{ik_{1,inc,j}x_p}+\left(\zeta_j+\mu_j i\right)e^{-ik_{1,ref,j}x_p}-B_{j,p}\right]^* + W_{j,p}\left[\left(\alpha_j+\gamma_j i\right)ix_p e^{ik_{1,inc,j}x_p}\right]^*\left[\left(\alpha_j+\gamma_j i\right)e^{ik_{1,inc,j}x_p}+\left(\zeta_j+\mu_j i\right)e^{-ik_{1,ref,j}x_p}-B_{j,p}\right] \tag{29}$$

$$\frac{\partial E}{\partial \zeta_j} = \sum_{p\in\mathbb{P}} W_{j,p} e^{-ik_{1,ref,j}x_p}\left[\left(\alpha_j+\gamma_j i\right)e^{ik_{1,inc,j}x_p}+\left(\zeta_j+\mu_j i\right)e^{-ik_{1,ref,j}x_p}-B_{j,p}\right]^* + W_{j,p}\left(e^{-ik_{1,ref,j}x_p}\right)^*\left[\left(\alpha_j+\gamma_j i\right)e^{ik_{1,inc,j}x_p}+\left(\zeta_j+\mu_j i\right)e^{-ik_{1,ref,j}x_p}-B_{j,p}\right] \tag{30}$$

$$\frac{\partial E}{\partial \mu_j} = \sum_{p\in\mathbb{P}} W_{j,p} ie^{-ik_{1,ref,j}x_p}\left[\left(\alpha_j+\gamma_j i\right)e^{ik_{1,inc,j}x_p}+\left(\zeta_j+\mu_j i\right)e^{-ik_{1,ref,j}x_p}-B_{j,p}\right]^* + W_{j,p}\left(-ie^{ik_{1,ref,j}x_p}\right)^*\left[\left(\alpha_j+\gamma_j i\right)e^{ik_{1,inc,j}x_p}+\left(\zeta_j+\mu_j i\right)e^{-ik_{1,ref,j}x_p}-B_{j,p}\right] \tag{31}$$

$$\frac{\partial E}{\partial k_{1,ref,j}} = \sum_{p\in\mathbb{P}} W_{j,p}\left[-\left(\zeta_j+\mu_j i\right)ix_p e^{-ik_{1,ref,j}x_p}\right]\left[\left(\alpha_j+\gamma_j i\right)e^{ik_{1,inc,j}x_p}+\left(\zeta_j+\mu_j i\right)e^{-ik_{1,ref,j}x_p}-B_{j,p}\right]^* + W_{j,p}\left[-\left(\zeta_j+\mu_j i\right)ix_p e^{-ik_{1,ref,j}x_p}\right]^*\left[\left(\alpha_j+\gamma_j i\right)e^{ik_{1,inc,j}x_p}+\left(\zeta_j+\mu_j i\right)e^{-ik_{1,ref,j}x_p}-B_{j,p}\right] \tag{32}$$

Using the exact gradient as defined above leads to a more robust optimization process and improves convergence behaviour. For the implemented problem the use of exact derivatives rather than the numerical approximations resulted in reductions in computational time on the order of 40 times. It should be noted that the exact gradients were verified against a numerical differentiation scheme prior to implementation in order to ensure correctness.

It is important to note that implemented decision variables, objectives, and the gradient of the objective are all real valued. Though the objective and gradient of the objective contain complex operations, these result in a real, thereby allowing IPOPT to be deployed. The Jacobian, the first derivative of the constraint equations, is simpler to formulate as the only non-bound constraint, which imposes that the wavenumbers must increase with frequency, is linear. As the constraint is linear, the Jacobian is constant and must only be evaluated once during the optimization process.

IPOPT which is distributed as part of the COIN-OR project (Lougee-Heimer, 2003) is distributed with a Matlab interface which has been used here to execute the optimization process.

4. Test Plan & Set-up

The conditions used to test and validate the presented methodology are detailed in Section 4.1, whilst the experimental configuration is described in Section 4.2.

4.1. Test Plan

Five sea states, based on Pierson-Moskowitz (PM) spectra, were chosen for generation in seven current velocities; totalling 35 experiments. These sea states are typical of those tested at the FloWave Ocean Energy Research Facility (see Section 4.2.1), having recently been used as part of an extensive and standardized test programme for Wave Energy Scotland (Highlands and Islands Enterprise, 2017). These sea states also cover a wide range of peak frequency, f_p. As wave-current interaction is highly frequency dependent, this enables a more detailed assessment of the method performance to wave-current combinations. These sea states have also been used in Draycott et al. (2018), where the incident and reflected wave systems were isolated by a more simplistic method utilising assumed current velocities and wavenumbers, and can be used as a useful benchmark for the presented, more advanced, methodology. The 5 sea states are given in Table 1.

Table 1: Matrix of wave test parameters

Sea State	H_{m0} [m]	f_p [Hz]
1	0.075	0.30
2	0.100	0.35
3	0.175	0.40
4	0.175	0.49
5	0.125	0.58

Each of the sea states were generated in current velocities of -0.3, -0.2, -0.1, 0, 0.1, 0.2 and 0.3 m s^{-1}. Current drive speeds were set based on a depth averaged calibration from measurements taken in the centre of the tank (as depicted in Sutherland et al. (2017)).

4.2. Experimental Configuration

4.2.1. The FloWave Ocean Energy Research Facility

All experimental measurements presented here were obtained at the FloWave Ocean Energy Research Facility (Fig. 3), Edinburgh, UK (Draycott et al., 2016). The 25 m diameter circular combined wave and current basin is encircled by 168 active-absorbing force-feedback wavemakers and has a nominal water depth of 2.0 m when wavemakers are in use. A re-circulating flow system is installed in the plenum chamber beneath the floor, utilising 28 impeller units (Robinson et al., 2015). This system enables a predominantly straight flow to be achieved in any direction across a central test area (Noble et al., 2015), where waves can additionally be added to the current field at arbitrary angles. This facility is therefore ideal for testing the presented wave-current solver.

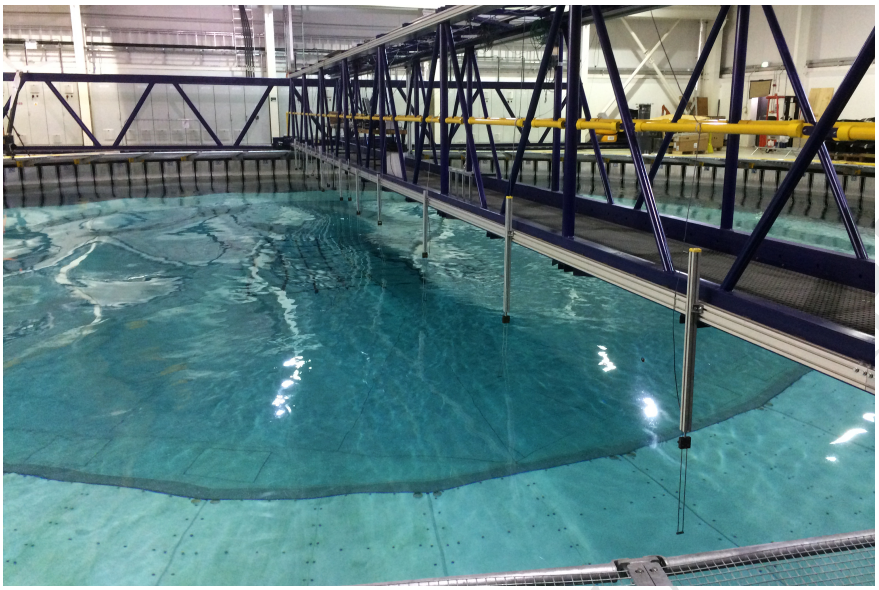

Figure 3: The FloWave Ocean Energy Research Facility

4.2.2. Instrumentation

A linear wave gauge array has been deployed comprising of nine resistance-type wave gauges. This array layout is based on an eighth order Golomb ruler (see Meyer and Papakonstantinou (2009)), providing desirable co-array properties suitable for reflection analysis (Draycott, 2017). The length of the array is 1.84 m long, providing useful separations for the frequency range of interest, and has been mounted about the tank centre (spanning −0.92 m to 0.92 m). An additional gauge at $x = 0$ has been added to obtain the centre-of-tank time-series.

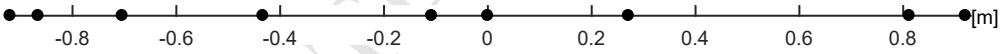

Figure 4: Reflection array based on eighth order Golomb ruler (Draycott et al., 2018)

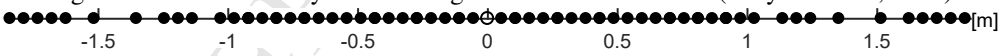

Figure 5: Co-array of Golomb ruler based reflection array (Draycott et al., 2018)

The array design along with the resulting co-array separations are shown in Figs. 4 and 5. The separations are extremely uniform, and thus provide excellent coverage over the spatial range of interest corresponding to the wavelengths present in the tank. This then provides a large number of useful separations, given as $0.05\lambda_i < \Delta x < 0.45\lambda_i$ in Goda and Suzuki (1976), over a wide range of frequencies.

5. Results

5.1. Optimization Performance

For each of the sea states given in Table 1, IPOPT was executed to minimize the error function as given in the optimization problem formulation. Each of these cases used IPOPT's internal non-

linear scaling methods to scale the problem such that the objective, gradient, and Jacobian were all approximately within a range between 1 and 100 as suggested in Wächter et al. (2015). This scaling allows both better convergence properties of the problem, as well as allowing better performance during the *restoration* phase of the algorithm (for more details on the phases of IPOPT see Wächter and Biegler (2006)).

IPOPT was set to terminate either once a maximum number of iterations (1,000,000) was reached or once the standard convergence criteria given by Wächter et al. (2015) were reached. For all 35 sea states considered, the maximum number of iterations was never reached, and the solutions reached the required convergence tolerances in between 57 and 100,000 iterations depending on the case. As IPOPT is a trajectory based algorithm, the initial solution given in Table 2 was supplied for each frequency component, j, at the start of the optimization process. Consistently, the cases with no current converged most quickly, in part due to the initial point for the wavenumbers being the current unmodified wavenumber. All solutions presented represent local optima, and in many cases are approximately equivalent to the global optima. Figure 6 shows the converged objective values for each of the simulations. For all cases, the error between the fit parameters and the gauge measurements were below 2×10^{-9} indicating that the converged solutions represent an accurate, low-error, estimate of the parameters of the wave systems.

Table 2: Optimization Initial Solution

Decision Variable	Initial Value
α_j	0.10
γ_j	0.01
ζ_j	0.10
μ_j	0.01
$k_{1,inc,j}$	$k_{0,j}$
$k_{1,ref,j}$	$k_{0,j}$

5.2. Isolated Incident and Reflected Wave Systems

Each of the five irregular wave cases defined in Table 1 have been recreated for each of the seven current velocities. Isolating the respective incident and reflected spectra produces the results presented in Figs. 7 to 9 with Fig. 7 showing the incident spectra and Figs. 8 and 9 depicting the reflected spectra in current following waves and current opposing waves respectively. The form of the incident spectra are generally as expected, and appear as a current-modified version of the PM input spectra. This indicates that, in these instances, the two wave systems have been well isolated; which tends to be particularly true for cases with low peak frequencies, in following current, or both.

The effective isolation of the wave systems when the dominant, incident, wave system is propagating against larger currents appears more problematic. It stands to reason that this is a result of turbulence. These turbulent velocity perturbations become a significant proportion of the group velocity of the waves, due to group velocities decreasing for waves opposing a current (Jonsson, 1990). This results in current modified wavenumbers and amplitudes which vary temporally, and

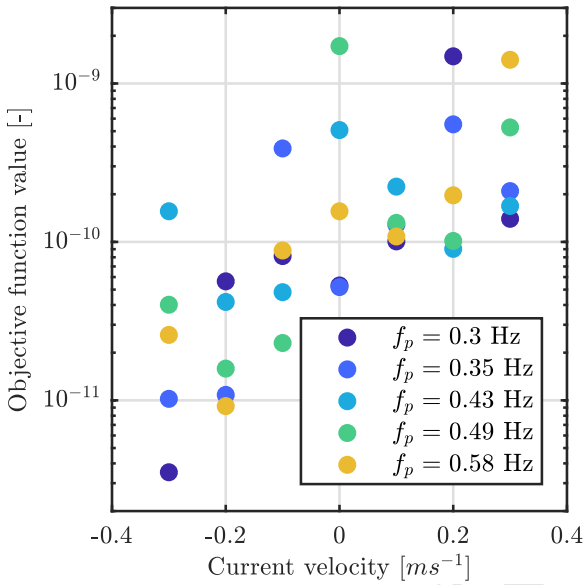

Figure 6: Converged objective function values for each of the 35 experiments.

are not stationary as assumed in the frequency domain analysis approach. This effect will worsen in higher opposing flows with a fixed turbulence intensity (TI), or with increasing TI, and will introduce slight errors in the isolated wave spectra, along with estimation of wavenumbers. This highlights an inherent limitation in using frequency domain approaches for non-stationary turbulent conditions.

A major capability of the methodology developed in this work compared to existing methods such as those presented in Draycott et al. (2018) is that in the general formulation, no prior knowledge regarding the current velocity or wavenumber is required to isolate the wave systems. This advantage leads to a greater degree of applicability and flexibility in this new methodology, and for this example enables the estimation of current velocity from the computed wavenumbers. Figure 10 illustrates the wavenumbers identified by this method for one of the sea states produced at FloWave. As indicated in this figure, the wavenumbers for the system following the current is subdued compared to k_0, the current unaffected wavenumber, while the wavenumber for the wave system opposing the current is elevated. This is consistent with linear and second order wave theory, as illustrated in Fig. 1. Compared to the theoretical values for this case, both parameters are well estimated, though the values for $k_{1,inc}$ are better estimated due to the current following this wave system.

5.2.1. Comparison to Draycott et al. (2018)

Comparing the results of the present methodology with those from Draycott et al. (2018) the presented method has low errors in estimating both the incident and reflected wave spectra and high correlation to the methodology outlined in Draycott et al. (2018). The wavenumbers, however, are characterized by higher errors and therefore lower coefficients of determination, in particular for the system opposing the direction of the current (see Table 3). As has been discussed previously,

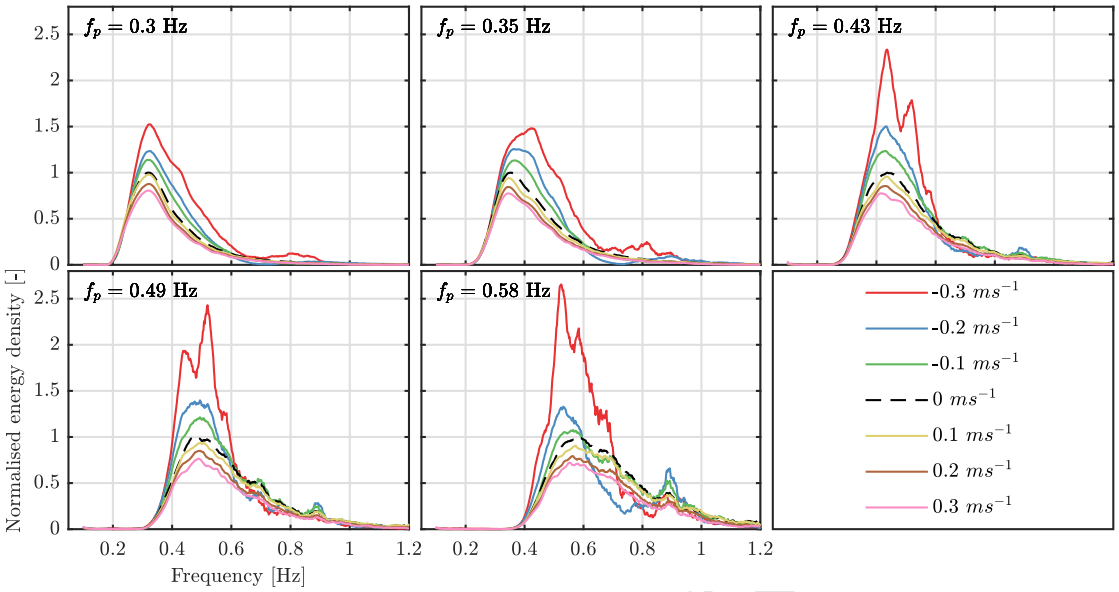

Figure 7: Incident frequency spectra for five PM spectra of differing peak frequency. The data are calculated for spectra created in currents ranging from $-0.3\,\mathrm{m\,s^{-1}}$ to $0.3\,\mathrm{m\,s^{-1}}$.

the methodology in general is more robust for isolating dominant wave systems following current rather than opposing them. This is further supported by the coefficients of determination presented in Table 3 comparing the parameters estimated using IPOPT against those identified in Draycott et al. (2018). From these results it can be observed that in the case of no current, IPOPT correctly identifies the same values of all parameters. In the presence of current, however, these values differ from the theoretical/calculated equivalents, yet good correlations are still found. The parameters of the wave systems following current display greater correlation than those for current opposing waves.

Table 3: Coefficients of determination between parameters estimated using IPOPT and those found in Draycott et al. (2018). The terms "following" and "opposing" refer to the direction of the incident wave system relative to the current.

Parameter	Following	Opposing	No Current	Overall
$k_{1,inc}$	0.98	0.91	1.00	0.89
$k_{1,ref}$	0.86	0.96	1.00	0.87
$S_{f,inc}$	0.99	0.98	1.00	0.98
$S_{f,ref}$	0.99	0.77	1.00	0.90
a_{inc}	0.99	0.99	1.00	0.99
a_{ref}	0.98	0.83	1.00	0.93

5.3. Isolated Incident and Reflected Time-Series

In addition to resolving the incident and reflected spectra, as shown in Section 5.2, it is also possible to reconstruct the incident and reflected time series of surface elevation. This is owed to

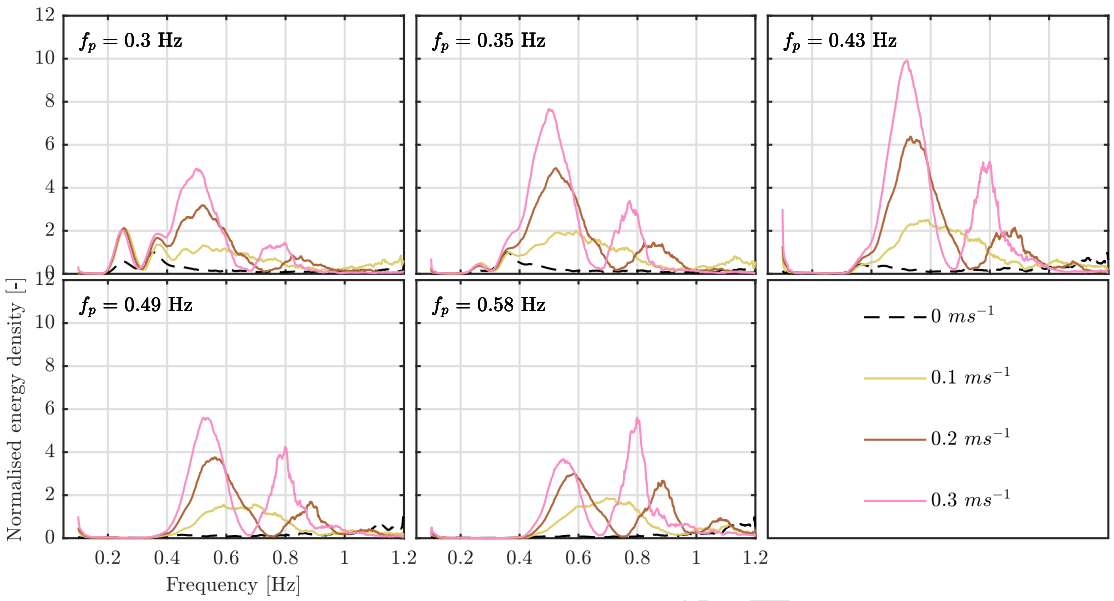

Figure 8: Reflected frequency spectra for waves following current. The data are shown for five PM spectra of differing peak frequency in currents ranging from $-0.3\,\mathrm{m\,s^{-1}}$ to $0.3\,\mathrm{m\,s^{-1}}$.

the phase-resolved solution approach, enabling the time-series of the two systems to be inferred. For the incident and reflected systems this can be calculated via an Inverse Fast Fourier Transform (IFFT) at a specified x location using Eqs. (33) and (34) respectively.

$$\eta_{inc,x} = \mathcal{F}^{-1}(a_{inc,j}e^{ik_{1,inc,j}x}) \tag{33}$$

$$\eta_{ref,x} = \mathcal{F}^{-1}(a_{ref,j}e^{-ik_{1,ref,j}x}) \tag{34}$$

where $\mathcal{F}^{-1}$ represents an IFFT.

An example of the isolated incident and reflected time-series at $x = 0$ is provided in Fig. 11 for the $f_p = 0.4922\ Hz$, $0.20\,\mathrm{m\,s^{-1}}$ following current case. Although the reflected time-series appears relatively small for this example, the time-total time-series is significantly altered and there are instances where the reflected system will dominate loads and response of any engineering system being tested (e.g. around 133 s). The largest peaks and troughs are also altered significantly from those expected from the incident spectrum alone, and will hence alter maximum loads experienced in such conditions. This highlights the requirement to understand the nature of the conditions being tested within, particularly as a device may respond very differently to opposing and following wave systems; either due to their relative orientation or the difference in wave kinematics.

5.4. Estimating Current Velocity

Once the optimization process was completed, the total representative current velocity, the weighted current velocity in the vertical region where the wave and current interact, for each experiment was estimated using Eq. (11) applied to the dominant wave system in each case. The results of this are shown in Fig. 12 for each of the wave spectra in each current velocity. As

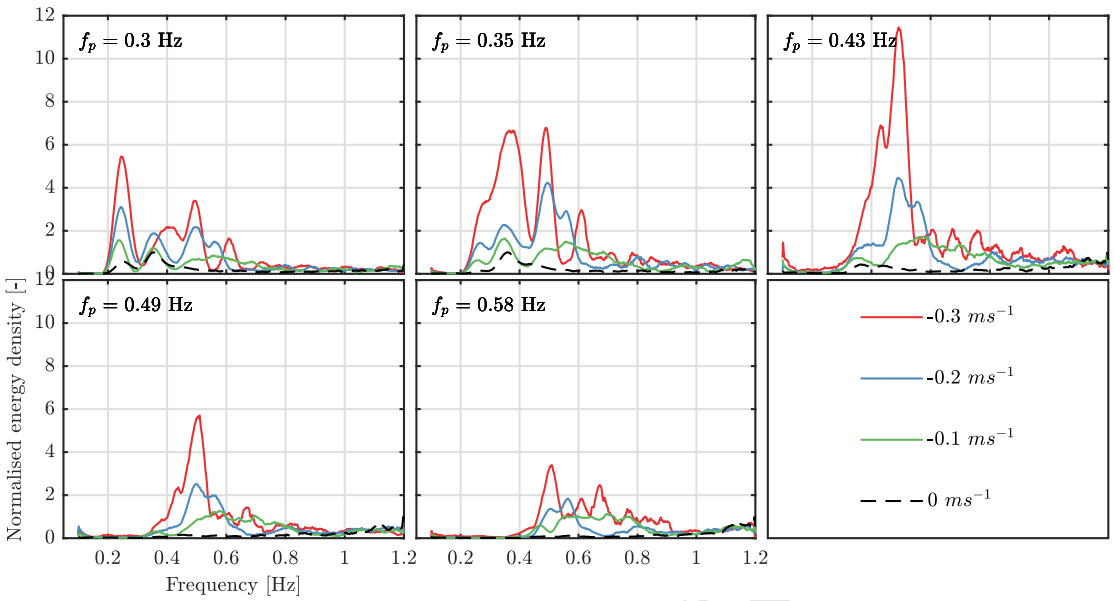

Figure 9: Reflected frequency spectra for waves opposing current. The data are shown for five PM spectra of differing peak frequency in currents ranging from $-0.3\,\mathrm{m\,s^{-1}}$ to $0.3\,\mathrm{m\,s^{-1}}$.

can be seen in this figure, in general, the current velocities are reasonably well estimated with a coefficient of determination of 0.99 and a root-mean-square-error of $0.031\,\mathrm{m\,s^{-1}}$. Though high correlation was observed between the estimated and true current velocities, there did appear to be a consistent overestimation of current speeds as indicated in Fig. 12. Better current estimates were observed for the cases of waves following current, with the cases in which the dominant wave system oppose the current resulting in a higher variation in current velocities. This is likely as a result in the greater difficulty in resolving the systems under these conditions. In general, for the cases where the dominant wave system was following the current, the magnitude of the current velocities were over-predicted and in the cases where the dominant wave system was opposing the current, the magnitudes were under-predicted. It is not entirely clear why this consistent behaviour was observed rather than the error being uniformly distributed. Whether this is a result of errors in the estimation of the parameters or if this is a real effect as a result of non-linear phenomena such as a net Stokes drift velocity, or alteration to mean current resulting from wave-current interaction (e.g. Kemp and Simons (1982); Olabarrieta et al. (2010)) remains unknown at present. It is, however, not thought to be a result of vertical shear, as this would provide an over-estimation (relative to depth averaged velocity) of the velocity magnitude for both following and opposing cases.

6. Discussion & Further Work

6.1. Additional Discussion of Results

The presented methodology has demonstrated its capabilities in estimating the parameters of wave systems and inferring current velocity for collinear systems utilizing a series of wave gauges

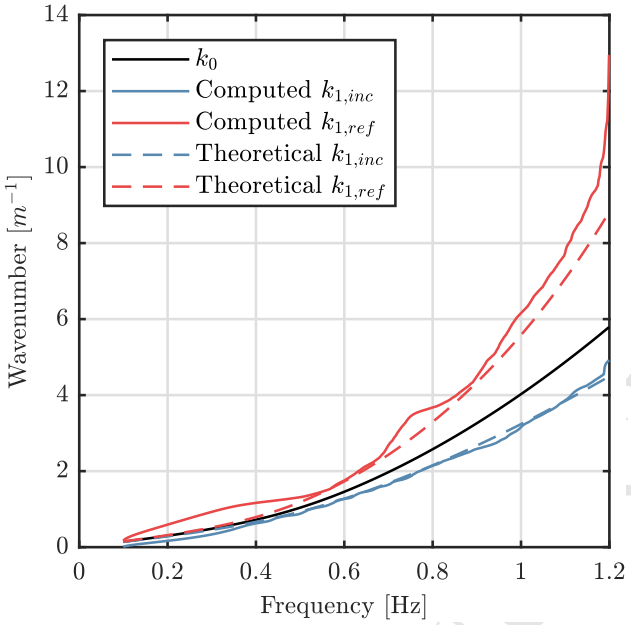

Figure 10: Wave numbers for current following waves, $f_p = 0.4922\ Hz$, $0.20\,\mathrm{m\,s^{-1}}$ current following waves.

in a linear configuration. This new method for resolving complex seas requires fewer assumptions than competing methods by virtue of solving for the current affected wavenumbers and is capable of delivering reliable results. The deployment of IPOPT, a gradient based optimization algorithm, has proven to be an effective means of isolating the collinear wave systems in the presence of current with high coefficients of determination compared to the simpler methodology from Draycott et al. (2018). The results presented in Figs. 7 to 9, have indicated that the methodology is more effective at characterizing the dominant wave system in following conditions at low peak frequency of the PM spectra. The secondary wave system, the reflected spectra in the experimental work, was not as smoothly defined especially in conditions where the dominant wave system (the incident spectra) were opposing the current. The expected form of the reflected system is, however, unknown and as such the true error is somewhat difficult to quantify.

The initial solution for the optimization shown in Table 2 were initially selected as they represented a reasonable first guess from which the optimizer could execute. The complex amplitudes were left relatively small with a more significant contribution from the real component than the imaginary component, and the wavenumbers were initialized to their current unaffected values. Further tuning of the initial solution could in principle improve the quality of the solutions and approach the global optima. An initial sensitivity study conducted after obtaining the presented results has indicated that an initial point for the wavenumbers being the current unmodified wavenumbers is the effective choice, and can be implemented without any prior knowledge of the current velocity or direction other than that it is colinear to the wave fields. This is shown in Fig. 13. From this figure it can be observed that there is little spread in the wavenumber for the following system (solid line) indicating that this is relatively insensitive to the initialization while the values for wavenumbers of the opposing wave system (dashed lines) are more sensitive.

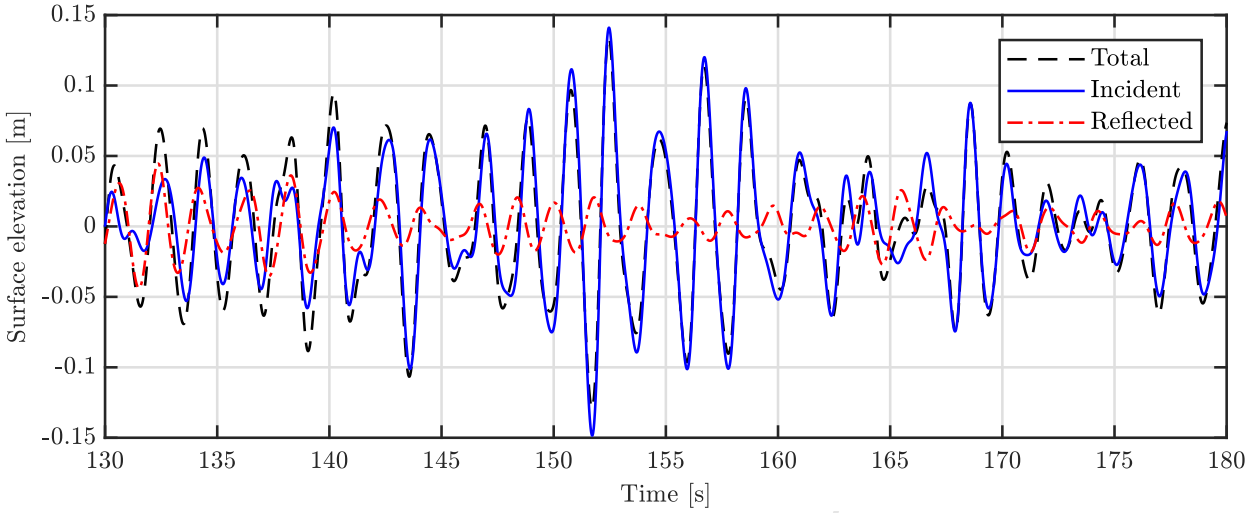

Figure 11: Example of time-series reconstruction of incident, reflected and total surface elevations. Shown for f_p = 0.4922 Hz, 0.20 m s^{-1} current following waves at $x = 0$

Though different initialization parameters are better for each of the individual wavenumbers, the initialization as the current unmodified wavenumbers for both results in the closest pair of curves when compared to the theoretical values shown in black on the plot supporting this selection of an initial solution.

Interestingly, the wave systems opposing the current ($k_{1,ref}$ in Fig. 13) indicates a dramatic over-prediction for frequencies exceeding 0.70 Hz for most initialization points. Due to the constraints requiring that the wavenumbers increase with frequency, this error once introduced around 0.70 Hz contributes to the higher errors in the remaining frequencies. This constraint has been introduced as without a similar constraint it was found that the wavenumbers identified by the optimization were highly volatile and did not represent feasible wavenumbers, as a smooth function over the frequencies would be expected. Introducing the constraint reduced the volatility, however, it also introduced this discrepancy in the wavenumbers if the initial point was not well selected. The high frequencies above the peak frequency of the spectra where this error is present is characterized by complex amplitudes which are low and in turn have low contributions to the objective function. This, therefore, makes it more challenging for the optimizer to converge effectively as it is difficult to distinguish between different solutions in the objective space. An alternative error function could therefore be explored. Preliminary transformations by looking at the logarithm of the error in order to inflate small changes in the error function and allow the optimizer to better differentiate between small changes in error led to a non-convex function with asymptotic behaviour which therefore did not have a well defined derivative. Alternate transformations could therefore be explored in future work if the error in the objective function are thought to be too large.

A similar sensitivity study on the initial point for the amplitudes yielded no discernible change in the final solution, but had a greater impact on the rate of convergence.

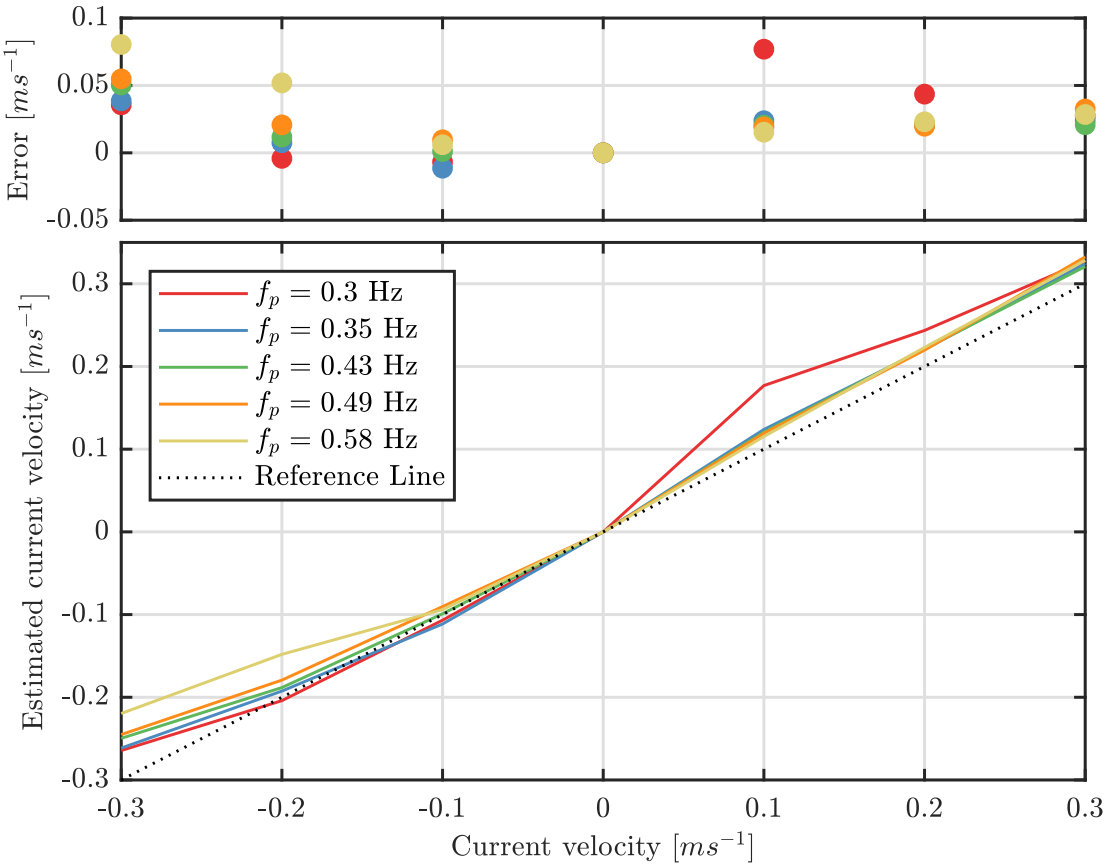

Figure 12: Error and correlation in estimated current velocities for five PM spectra of differing peak frequency. The data are calculated for spectra created in currents ranging from −0.3 m/s to 0.3 m/s. R^2 = 0.99 and RMSE = 0.031 m s^{-1}.

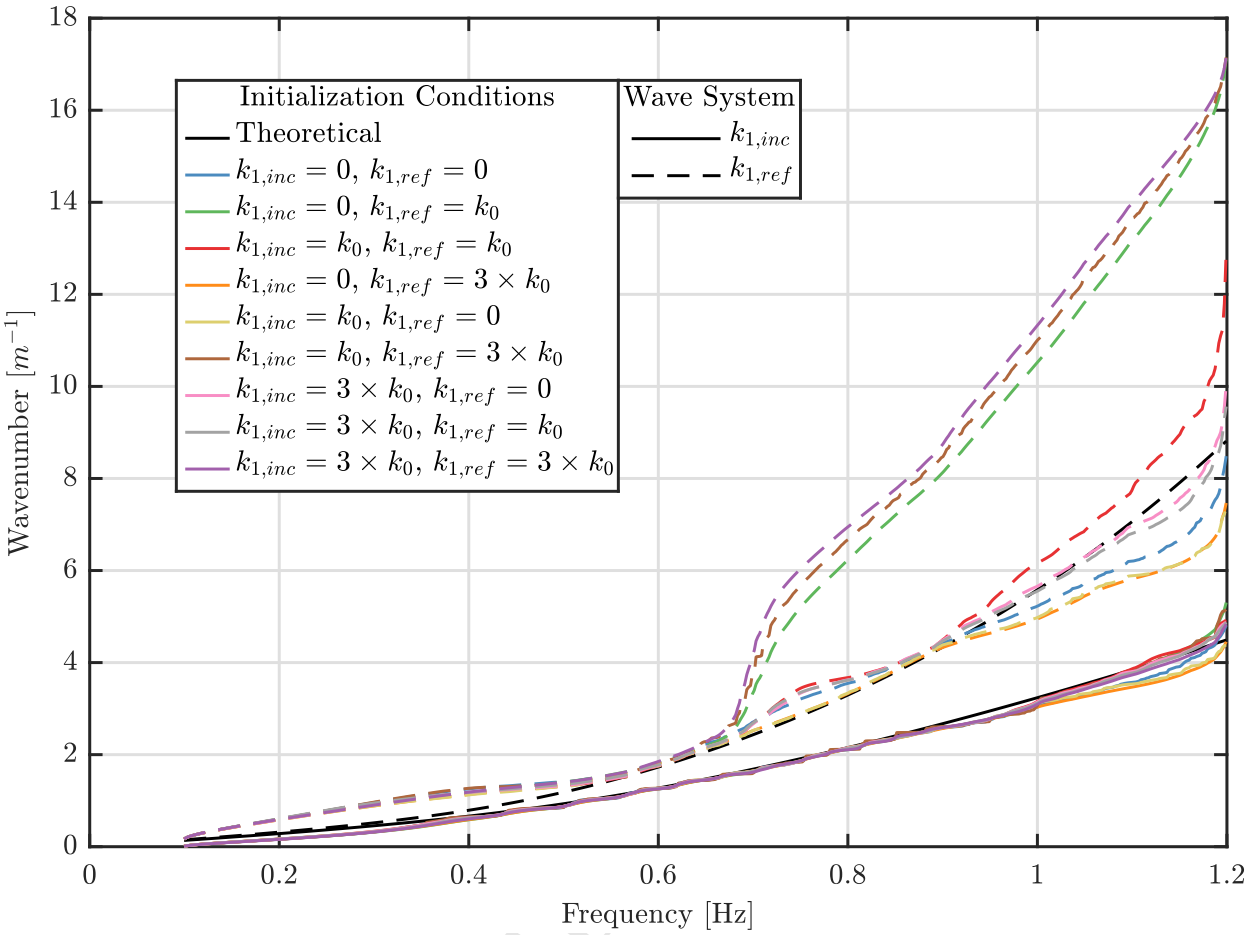

Figure 13: Sensitivity to initialization of wavenumbers in IPOPT for current following waves, $f_p = 0.4922\ Hz$, $0.20\ \mathrm{m\,s^{-1}}$ current following waves.

6.2. *Future Work*

The results presented here considering two wave systems in the presence of current is of direct value to scale testing in combined wave and current tanks such as FloWave, however, the methodology is extendible to any number of wave systems as long as the wave gauge arrangement ensures that the system is over-resolved. A trivial extension of this method by introducing additional parameters can solve for the parameters of non-collinear systems. This straightforward increase in complexity of the solution method can provide valuable insights, resolving for angle and identifying refraction effects. Both solving such a system and the experimental set-up will be more challenging, as the increase in decision variables to the optimization problem will significantly increase the computational complexity, while ensuring that the system is over-resolved will require many wave gauges in a two-dimensional arrangement. In general, the present framework should be capable of solving any characterization or isolating problem regardless of complexity, as long as sufficient wave gauges are deployed at the correct separations in order to ensure that the system is over-resolved. Hence, future work will aim to test and demonstrate the presented

methodology to resolve multiple directional wave fields with and without the presence of current.

Importantly, it should also be noted that though the Fourier coefficients of the sea surface elevation was explored in the numerical and experimental work presented here, the same formulation and solution approach can be used with few changes in order to solve for the Fourier coefficients or parameters which define any wave signal. This will be particularly valuable for applications with ocean data where acoustic, Doppler-based, velocity instruments and pressure sensors are often deployed in tidal channels. This potentially enables a significant amount of additional information to be inferred from existing metocean datasets, and will be explored as an exciting area of future research.

7. Conclusions

This paper has presented a novel methodology utilizing interior point optimization to resolve and characterize multiple wave systems in the presence of current. Addressing the parameter estimation problem as an error minimization problem, IPOPT can successfully resolve the incident and reflected wave systems in the frequency domain identifying the complex amplitudes and wavenumbers. The numerical procedure is demonstrated to be effective at resolving incident and reflected wave systems propagating in opposite directions on a current field, for a range of waves and current velocities tested at the FloWave Ocean Energy Research Facility. The isolation of wave systems proved consistent with a previous simplified method (Draycott et al., 2018) with coefficients of determination exceeding 0.87 for the wave system parameters, whilst additionally providing estimates of wavenumber and current velocity. The application of this methodology requires fewer assumptions than existing methods and is therefore capable of solving more complex wave systems. An initial sensitivity study has indicated that this methodology is sensitive to the initial solution in particular the wavenumber and the quality of the estimate can be improved through the more accurate selection of an initial solution.

The developed method preserves phase information, resulting in the ability to reconstruct the time-series of the two wave systems; providing valuable additional information. With the proper consideration and effective wave gauge separations the presented numerical framework has the potential to resolve a wide range of complex wave and wave-current combinations thus improving the understanding of these conditions for engineering design.

Future extensions of this framework will explore the application of this methodology to more complex wave systems including non-collinear systems as well as utilizing additional experiments from physical testing in order to improve the initial solutions, and the guidelines for selecting these.

Acknowledgements

The authors would like to thank the Energy Technologies Institute and RCUK Energy programme for funding IDCORE programme (EP/J500847/1) where this research originally emanated and the collaborations were initiated. In addition the authors would like to recognize the UK EPSRC for funding the FloWave Ocean Energy Research facility (EP/I02932X/1). The UK EPSRC is further acknowledged for supporting A.C. Pillai through the United Kingdom Centre for Marine Energy Research (UKCMER) (EP/P008682/1).

References

Benoit, M., Frigaard, P., Schaffer, H. A., 1997. Analyzing multidirectional wave spectra: a tentative classification of available methods. Proceedings of the 1997 IAHR conference, 131–158.

Bruserud, K., Haver, S., Myrhaug, D., 2018. Joint description of waves and currents applied in a simplified load case. Marine Structures 58 (4035), 416–433.
URL https://doi.org/10.1016/j.marstruc.2017.12.010

Burke, E. K., Kendall, G., 2013. Search Methodologies, 2nd Edition. Springer US, Boston, MA.

Chen, H. B., Tsai, C. P., Chiu, J. R., 2006. Wave reflection from vertical breakwater with porous structure. Ocean Engineering 33 (13), 1705–1717.

De Dominicis, M., O'Hara Murray, R., Wolf, J., 2017. Multi-scale ocean response to a large tidal stream turbine array. Renewable Energy 114, 1160–1179.
URL http://dx.doi.org/10.1016/j.renene.2017.07.058

Dickson, W., Herbers, T., Thornton, E., 1995. Wave Reflection From Breakwater 121 (October), 262–268.

Draycott, S., 2017. On the Re-creation of Site-Specific Directional Wave Conditions. Ph.D. thesis, The Universities of Edinburgh, Strathclyde and Exeter.

Draycott, S., Davey, T., Ingram, D. M., Day, A., Johanning, L., 2016. The SPAIR method: Isolating incident and reflected directional wave spectra in multidirectional wave basins. Coastal Engineering 114, 265–283.

Draycott, S., Steynor, J., Davey, T., Ingram, D. M., 2018. Isolating incident and reflected wave spectra in the presence of current. Coastal Engineering Journal, 1–12.

Goda, Y., Suzuki, T., 1976. Estimation of incident and reflected waves in random wave experiments. Coastal Engineering Proceedings 1 (15).

Highlands and Islands Enterprise, 2017. Wave Energy Scotland.
URL http://www.hie.co.uk/growth-sectors/energy/wave-energy-scotland/

Ingram, D., Wallace, R., Robinson, A., Bryden, I., 2014. The design and commissioning of the first, circular, combined current and wave test basin. Oceans 2014 - Taipei.

Jefferys, E., 1987. Directional seas should be ergodic. Applied Ocean Research 9 (4), 186 – 191.
URL http://www.sciencedirect.com/science/article/pii/0141118787900010

Jonsson, 1970. Interaction between Waves and Currents.

Jonsson, I. G., 1990. Wave-current Interactions. In: LeMehaute, B., Hanes, D. M. (Eds.), The Sea, Ocean Engineering Science. Vol. 9. Wiley-Interscience publications, New York, Ch. 7, pp. 65–120.

Kemp, P. H., Simons, R. R., apr 1982. The interaction between waves and a turbulent current: waves propagating with the current. Journal of Fluid Mechanics 116, 227–250.

Krogstad, H. E., 2000. Linear Wave Theory Random Waves and Wave Statistics (February).

Lougee-Heimer, R., 01 2003. The common optimization interface for operations research: Promoting open-source software in the operations research community. IBM Journal of Research and Development 47 (1), 57–66, copyright - Copyright International Business Machines Corporation Jan 2003; Last updated - 2017-10-31; CODEN - IBMJAE.
URL https://search.proquest.com/docview/220690110?accountid=10792

Masson, D., 1996. A case study of wave-current interaction in a strong tidal current.

Meyer, C., Papakonstantinou, P. A., 2009. On the complexity of constructing Golomb Rulers. Discrete Applied Mathematics 157 (4), 738–748.

Miles, M. D., Funke, E. R., 1989. A Comparison of Methods for Synthesis of Directional Seas.

Noble, D. R., Davey, T., Smith, H. C. M., Kaklis, P., Robinson, A., Bruce, T., 2015. Characterisation of spatial variation in currents generated in the FloWave Ocean Energy Research Facility. In: 11th European Wave and Tidal Energy Conference, Nantes, France. Nantes, France, pp. 1–8.

Olabarrieta, M., Medina, R., Castanedo, S., 2010. Effects of wave-current interaction on the current profile. Coastal Engineering 57 (7), 643–655.
URL http://dx.doi.org/10.1016/j.coastaleng.2010.02.003

Rao, S. S., 2009. Engineering Optimization: Theory and Practice, 4th Edition. John Wiley & Sons, Hoboken, New Jersey.

Robinson, A., Ingram, D., Bryden, I., Bruce, T., 2015. The generation of 3D flows in a combined current and wave tank. Ocean Engineering 93, 1–10.

Rodríguez, G., Guedes Soares, C., 1999. A criterion for the automatic identification of multimodal sea wave spectra. Applied Ocean Research 21 (6), 329–333.

Smith, J. M., 1997. One-dimensional wave-current interaction. Tech. Rep. 9, US Army Engineer Waterways Experiment Station, Coastal Engineering Research Center, Engineer Research and Development Center Vicksburg MS Coastal and Hydraulics Lab.

Sutherland, D. R. J., Noble, D. R., Steynor, J., Davey, T. A. D., Bruce, T., 2017. Characterisation of Current and Turbulence in the FloWave Ocean Energy Research Facility. Ocean Engineering 139 (May), 103–115.

Wächter, A., 2002. An Interior Point Algorithm for Large-Scale Nonlinear Optimization with Applications in Process Engineering. Doctor of philosophy dissertation, Carnegie Mellon University.

Wächter, A., Biegler, L., 2006. On the implementation of a interior point filter line search algorithm for large-scale nonlinear programming. Mathematical Programming 106, 25–57.

Wächter, A., Kawajir, Y., Laird, C. D., Vigerske, S., 2015. Introduction to IPOPT: A tutorial for downloading, installing, and using IPOPT . Tech. rep.

Wright, M. H., 2005. The interior-point revolution in optimization: History, recent developments, and lasting consequences. Bulletin of the American Mathematical Society 42 (1), 39–56.

Ye, Y., 1997. Interior-Point Algorithm: Theory and Analysis. Wiley-Interscience.

Zelt, J. a., Skjelbreia, J., 1992. Estimating Incident and Reflected Wave Fields Using an Arbitrary Number of Wave Gauges. Coastal Engineering Proceedings 1, 777–789.

- Frequency domain solver developed for resolving combined wave-current fields
- Wave gauge measurements from a circular combined wave-current tank utilized
- Method enables the isolation of wave systems and prediction of current velocity
- Low errors observed in estimates of incident and reflected spectra and wavenumbers
- Applicability to a wide range of complex wave and wave-current fields